Cooling of a heating cylinder by confined impacting air jets

Nicolas Chauchat, Éric Schall, Mathieu Mory, Marta de La Llave Plata, Vincent Couaillier

Cooling of a heating cylinder by confined impacting air jets

Nicolas Chauchat[1], Éric Schall[1], Mathieu Mory[1], Marta de la Llave Plata[2], Vincent Couaillier[2]
[1] UPPA - Université de Pau et des Pays de l'Adour
[2] ONERA – The French Aerospace Lab [Châtillon]

ABSTRACT

Future aircraft technology will increasingly rely on electrical power. The substitution of mechanical energy by electrical energy will lead to an increasing amount of heat power that need be evacuated. Innovative cooling processes have to be set up according to constraints imposed by the technological design. The present study, conducted within the framework of onboard aircraft, considers a new cooling system of a small turbo engine stator. The experimental facility, designed and built at Pau University, consists in air jets impacting around a heated circular cylinder. As the inlet velocity magnitude is low (V_{in}=4.37m/s - $Mach_{in}$=0.0125), using a compressible solver for numerical simulations presents a number of difficulties. For this low Mach number configuration, we compare in this paper the performance of three different solvers. Two of them are compressible, one based on the finite volume approach and the other on a discontinuous Galerkin method, and the third one is an incompressible solver. Some of the numerical results are compared to experimental data.

NOMENCLATURE

C_p	specific heat	$J.kg^{-1}.K^{-1}$
DG	discontinuous Galerkin method	(-)
H	R_e - R_i	m
k	air conductivity	$W.m^{-1}.K^{-1}$
$k^{(2)}$	second order dissipation coefficient	(-)
$k^{(4)}$	forth order dissipation coefficient	(-)
L	cylinder length	m
$\dot{m}$	mass flow rate	$kg.s^{-1}$
$Mach_{in}$	inlet Mach number	(-)
Oz	third axis	(-)
p	polynomial degree of the DG method	(-)
P	pressure	Pa
P_{conv}	thermal convective power	W
P_{elec}	electrical Power	W
q_i	local heat flux density	$W.m^{-2}$
R_i	internal radius	m
R_e	external radius	m
rms	root mean square	$m.s^{-1}$
S_f	slot width	m
T	temperature	K
T_{ex}	wall external temperature	K
T_i	inlet temperature	K
T_{in}	wall internal temperature	K
T_o	outlet temperature	K
u_i	velocity components	$m.s^{-1}$
V_{in}	inlet velocity	$m.s^{-1}$
x,y,z	spatial axis	m

x_i directional components ……...……m

Greek symbols

δ_{ij} Kronecker symbol ……..……..……(-)

ρ density ……..……$kg.m^{-3}$

τ_{ij} viscous stress tensor ……..……Pa

μ dynamic viscosity ……..…$kg.m^{-1}.s^{-1}$

1. INTRODUCTION AND CONTEXT

“Green aircraft projects” aim at reducing greenhouse gas emissions, pollutants and fuel consumption. The use of electrical systems in aircrafts is growing in all aeronautical programs for many reasons. Indeed, the “All-Electric E-Fan 2.0 Airplane” project by Airbus and the Boeing "Subsonic Ultra-Green Aircraft Research" (SUGAR) program investigate technologies that might allow the subsonic commercial aircrafts to meet environmental requirements in 2030 to 2050. Recent research like GREENAIR (7th RTD European framework programme) or the recent technological achievements on the A380 as on the Boeing 787 demonstrates that the use of electricity is increasing on-board. The use of electrical energy instead of mechanical energy is a challenge for aircraft equipment manufacturers. Electrical processes lead to an additional thermal charge that needs to be evacuated. Thus, dedicated new cooling system devices have to be developed. Up to now, for industrial applications, using air flow remains one of the best solutions for cooling electrical machines, while satisfying the objective of lower cost and weight.

This project has been partially supported by DGCIS* research funds (France) during four years, after having selected by the French cluster Aerospace Valley. The studied device is representative of any small turbo-engine and his potential for industrial applications is not restricted to aeronautics. Because of the high heat transfer coefficients occurring in the impingement region, cooling by air jet impingement is relevant to several engineering applications such as tempering of glass, cooling of turbine blades, drying of industrial goods and cooling of electronic chips. The physics of jet impingement flows is described in detail by the pioneering work by Gardon and Akfirat (1965). A circular or slot impinging jet on a flat plate serves as a fundamental configuration for many others. A number of studies are devoted to these configurations (Gardon and Akfirat, 1965, Martin, 1977, Jambunathan et al., 1992, Gardon and Akfirat, 1966, Zuckerman and Lior, 2006). Various nozzles used to generate impinging jets have been studied and reviewed. The effect of nozzle shape (circular or rectangular) on the heat transfer from a circular cylinder by impinging jets was studied recently (Singh et al., 2015) in experiments and numerical investigations. Similarly, applications of the impingement process on various target shapes are gaining popularity in industry. Though most reviews focus on the jet impingement cooling of flat surfaces, jet impingement research on circular cylinders is expanding, both for circular jets (Gori and Bossi, 2000, McDaniel and Webb, 2000) and slot jets (Singh et al., 2013, Sight et al., 2015, Wang et al., 2014. In (Zuckerman and Lior, 2007), numerical results from various models are compared against test data for flat-plane jet impingement heat transfer, and a numerical turbulent model based on accuracy is selected to perform jet impingement flows over a cylindrical target surface.

According to the authors' bibliographical study on jet impingement, three key points deserve special attention and are studied in this paper. The first one is the validation of 2D numerical simulations when compared to 3D ones. The second one is the accuracy of compressible simulations at low Mach number. This is addressed here by comparing the results of incompressible-oriented models and compressible-oriented models. Herein two compressible solvers are compared, a finite volume method and a high order finite element method. The third highlight deals with the comparison between numerical results and results of an experiment.

The cooling process studied herein is achieved by four normal (or radial) air jets, which impact on a heating cylinder (Fig. 1). The geometry is 2D. The cooling air is injected through four radial slots respectively oriented north, south, east and west. The confined fluid leaves the cylinder through four others radial slots shifted 45 degrees from the inlets.

A series of CFD simulations were performed using three different numerical methods. The inlet velocity was fixed to 4.37m/s, which correspond to an available data set. Two compressible solvers have been considered, namely the *elsA* solver based on a finite volume approach and the Aghora solver based on a discontinuous Galerkin method, as well as the incompressible solver of ANSYS-FLUENT. Indeed, even if the inlet Mach number is low ($Mach_{in}$=0.0125), the authors are not convinced that the fluid is devoid of any compressibility effect. It is also well known that the numerical resolution of the compressible set of the Navier-Stokes equations at very low Mach numbers is very sensitive to numerical errors, especially when a low-order discretization is used. We compare here the results provided by the *elsA* and Aghora models, for which the spatial order of accuracy is set to second order. For the Aghora solver, this implies setting the polynomial degree to 1 (p=1). We however note that the discontinuous Galerkin (DG) method ensures that the formal order of accuracy is 2 on irregular meshes as opposed to the finite volume approach, for which the order of accuracy is not preserved when irregular meshes are used. The comparison is made at the global level of the experimental facility and the level of the fluid particle. At the global level, the total convective heat flux and the mass balance in the cavity is considered. At the fluid particle level, the heat flux variations at the wall along the azimuthal direction and the streamlines pattern inside the cavity are studied.
The paper is organised as follows. The original set-up is described in section 2. The numerical methods used in the three softwares are presented in section 3. In section 4, the comparisons between numerical simulations and experiment are discussed. Finally, the last section addresses some of the main difficulties linked to the compressibility assumption for CFD simulations for complex geometries.

2. EXPERIMENTAL DESIGN

The experimental set-up achieves the cooling of the surface of a circular cylinder of radius R_i by 4 plane jets impacting perpendicularly the heated cylinder. As shown in Fig. 1, the four impacting jets are directed from the north, east, south and west, respectively. The heated air is extracted through four outlet slots, the directions of which are along the angle bisector between neighbouring inlet jets. The flow is confined in the annular domain with internal radius R_i=5.4cm and external radius R_e=7cm. The slot width is S_f=3.6mm. Numerical simulations were carried out assuming 2D flow, i.e. it does not vary in the direction Oz perpendicular to the cross-section shown in Fig. 1. The cylinder length is L=4.7cm in the experiment.

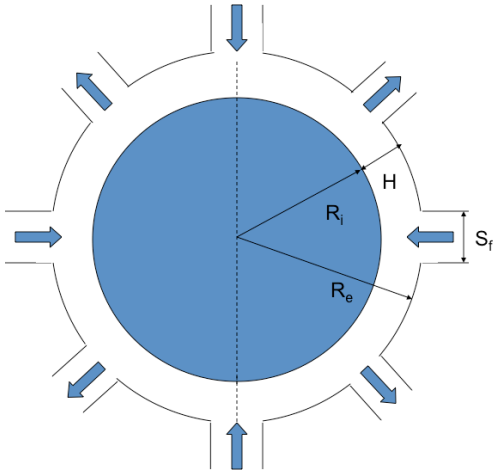

Figure 1. Cross-section of the cavity in which the flow cools the heated cylinder of radius R_i.

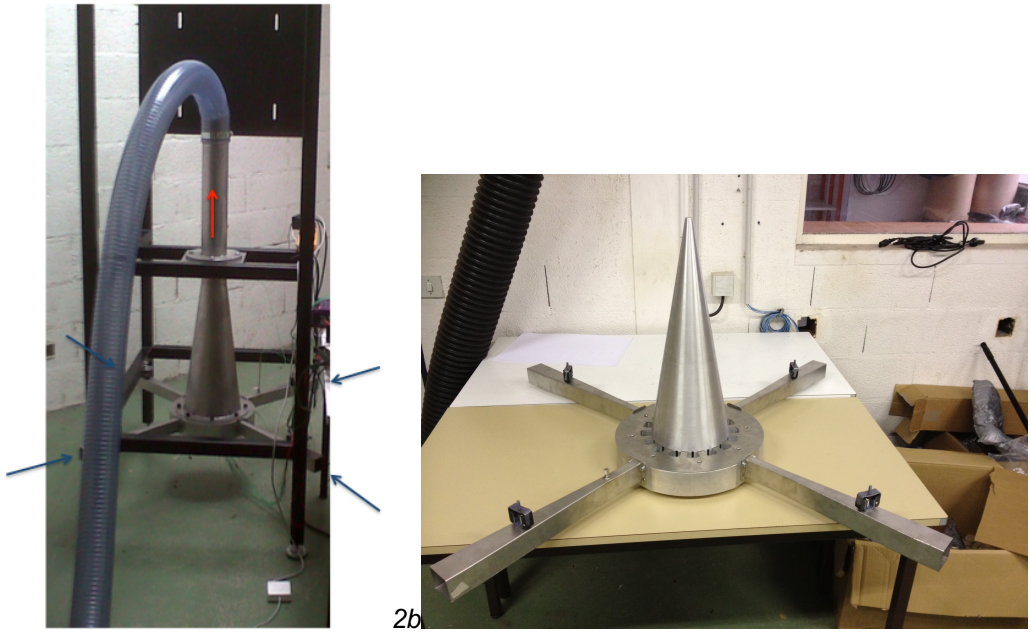

2a *2b*

Figure 2. Photographs of the experimental set-up.

The photograph in Fig. 2a shows the experimental set-up. The blue arrows indicate the flow into four rectangular tubes leading to the entrance slots into the cavity. The casing ensuring the inlet distribution of the jets impacting the cylinder and collecting the warm air outside the flow cavity is shown in Fig. 2b. The heated cylinder is inserted under the cone seen in Fig. 2b, which channels the exit warm air into the vertical tube seen in Fig. 2a. The red arrow indicates the direction of the outlet flow into a flexible tube, which is downstream connected to a mass flowmeter (Eldridge 9700MPNH), a fan and a vane.

The circular cylinder is heated using an electrical resistance inserted inside an adhesive polyamide mat glued over the inner surface of the cylinder (brown in Fig. 3a). The surface temperature on the cylinder is measured using thermocouples (type K). The thermocouples wires (green in Fig. 3a) traverse the mat and the cylinder (thickness 2mm) and the measuring extremities are bended after coming up to the cylinder surface. The entire surface of the cylinder is wrapped by an adhesive film (supporting high temperature), which maintains the thermocouples in contact with the cylinder. Fig. 3b shows an external view of the cylinder. The locations of the thermocouples are shown. The sketch at the bottom indicates that thermocouples 8, 9 and 12 are along the axis line of an impacting jet, whereas thermocouples 1, 10 and 11 are along the axis line of an outlet slot. The experimental conditions given by the mass flow rate and the electrical power P_{elec} result in a steady regime. The temperature variation at the surface of the cylinder, corresponds to the equilibrium of the furnished electrical power with the convective power extracted by the air and the conductive power transmitted through the aluminium casing.

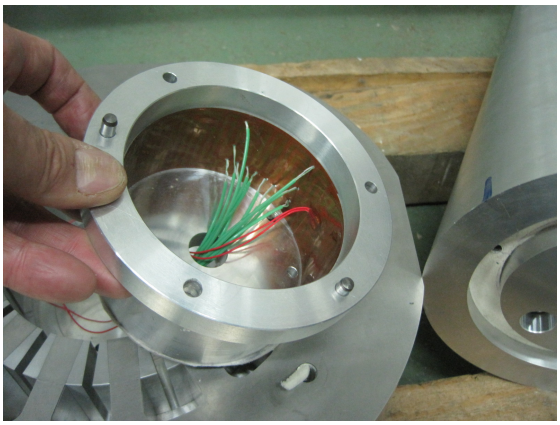

Figure 3a. Inside view of the heated cylinder.

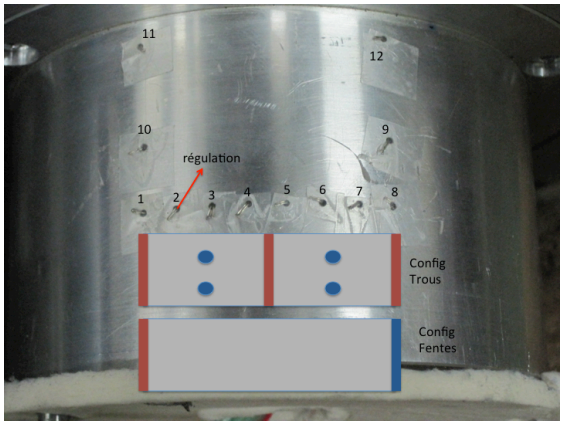

Figure 3b. Outside surface view of the heated cylinder showing the thermocouple positions.

The present paper focuses on a flow configuration at Reynolds numbers lower than 1100. For the experiments considered in this paper, the electrical power delivered was reduced to 212W as compared to the maximum electrical power (420W) in order to maintain the surface temperature less than 100°C (maximum temperature supported by the resistance polyamide mat). The electrical power delivered was measured using a wattmeter. The convective thermal power extracted by the air flow was estimated from the temperature difference measured by two thermocouples (type K), one being placed inside one of the inlet tube (T_i) and the other (T_o) at the exit of an outlet slot from the cavity. Estimating the thermal convective power, $P_{conv} = C_p \dot{m}\left(T_e - T_i\right)$, relies also on an accurate measurement of the mass flow rate of air m. The average surface temperature T_{in} was finally determined from thermocouple measurements on the cylinder surface.

The present paper mainly addresses the ability of different numerical models to determine the heat transfer, for moderate Reynolds number conditions. We basically compare, for a moderate Reynolds number, the convective thermal power P_{conv} and the temperature difference T_{in}-T_i, obtained from the different numerical simulations, with the experimental values.

Experimental limitations:

In this study the boundary conditions for CFD computations (velocity and temperature at the entrance, temperature at the surface of the heating cylinder) were stated from the laboratory experiment. Results of experiment and simulation are then compared considering the global convective heat transfer achieved. Because of its confinement, the experimental set-up does not provide access to the detailed flow and thermal properties that could be compared to the flow streamlines or the temperature variations all over the surface of the heated cylinder obtained from numerical simulations. Local measurements nevertheless show limited variations of temperature at the surface of the heated cylinder, indicating that a condition of uniform

parietal temperature of the cylinder is relevant. The temperature boundary conditions are fixed for the CFD computations using the experimental temperature data and the inlet flow velocity is determined from the mass flow rate measurement. The experiment also delivers the global convective power that is compared to the total convective power computed by the CFD simulations.

3. NUMERICAL METHODS AND SOFTWARES

This work investigates the differences between CFD computations of an engineering heat transfer flow, which primarily differ through the assumption that the fluid is incompressible or compressible. This requires knowledge in various disciplines (especially applied mathematics, physics and programming) in order to interpret the results of numerical solutions in full knowledge of their specificity and in order to compare with experimental results, trusting that the CFD simulates effectively the physical case of the experiment. When considering the compressible/incompressible nature of the fluid, the first step consists in fixing the modeling through the determination of the unknown variables and the set of partial differential equations (PDE) to solve. This step is challenging because the numerical resolution of the discretized form of PDE depends also on the nature of PDE considered.

Incompressible simulation by ANSYS-FLUENT:

Simulations for an incompressible fluid were carried using the ANSYS_FLUENT software (Kelecy, 2008). Simulating an air flow considered as incompressible is widely used in aeronautics. The ANSYS-FLUENT software was chosen, considering the experience of this software, both for incompressible and compressible fluids. For incompressible fluid, density is considered as constant. The unknown variables are reduced to vector (P, u, T) - respectively pressure, velocity and temperature -, which are determined from the conservation equations for mass (continuity), momentum and energy as follows in Einstein notation:

Continuity:

$$\frac{\partial u_i}{\partial x_i} = 0$$

Momentum:

$$\rho u_j \frac{\partial u_i}{\partial x_j} = -\frac{\partial P}{\partial x_i} + \mu \frac{\partial^2 u_i}{\partial x_j^2}$$

Energy:

$$\rho u_j C_p \frac{\delta T}{\delta x_i} = \mu u_j \frac{\delta^2 u_i}{\delta x_j^2} - \frac{\delta q_i}{\delta x_i}$$

u_i, ρ, T, P denote the velocity components, density, temperature and pressure, respectively. C_p and μ are the specific heat at constant pressure and the dynamic viscosity, respectively. x_j are the directional components and *t* is time. The local heat flux density is given by Fourier's law: $q_i = -k \frac{\partial T}{\partial x_i}$ (*k* is the thermal conductivity of air)

For an incompressible fluid, the relation of perfect gas is not used and the pressure is only velocity dependent. The pressure-based method has been selected and the SIMPLE and PISO algorithms have been both tested, in order to determine the pressure and velocity fields, via the zero-divergence of the velocity. The employed method is segregated, leading to regular corrections of the pressure along the iterative process. As the "steady" option is selected there is no time-marching in the calculation procedure of ANSYS-FLUENT. Finally, the temperature is deduced from the conservation equation of the energy written in terms of temperature and resolved alongside the other variables.

Compressible simulation by elsA and Aghora:

The *elsA* (Cambier et al., 2013) software is a multi-application CFD platform, dealing especially with internal and external aerodynamic flows, ranging from the low subsonic to the high supersonic regimes. *elsA* is the reference ONERA aerodynamics solver (see (Cambier et al., 2013) and <http://elsa.onera.fr> for a exhaustive review of accomplishments both from the research and industrial sides). The software is based on finite volume (FV) schemes for multi-bloc structured and unstructured meshes (Llave Plata et al., 2012). The set of PDE solved for compressible flows is given below in Einstein notation:

Continuity:

$$\frac{\partial \rho}{\partial t} + \frac{\partial \rho u_i}{\partial x_i} = 0$$

Momentum:

$$\frac{\partial \rho u_i}{\partial t} + \frac{\partial \rho u_i u_j}{\partial x_j} = -\frac{\partial P}{\partial x_i} + \frac{\partial \tau_{ij}}{\partial x_j}$$

with the viscous stress tensor

$$\tau_{ij} = \mu\left(\frac{\partial u_i}{\partial x_j} + \frac{\partial u_j}{\partial x_i}\right) - \frac{2}{3}\mu\left(\frac{\partial u_k}{\partial x_k}\right)\delta_{ij}$$

δ_{ij} is the Kronecker symbol (such that δ_{ij} is 1 if $i = j$ and 0 if $i \neq j$).

Energy:

$$\rho\frac{\partial}{\partial t}\left(C_v T + \frac{1}{2}\rho u^2\right) + \rho u_j \frac{\partial}{\partial x_j}\left(C_v T + \frac{1}{2}\rho u^2\right) = -\frac{\partial}{\partial x_i}\left(P u_i\right) + \frac{\partial}{\partial x_j}\left(\tau_{ij} u_i\right) - \frac{\partial q_i}{\partial x_i}$$

u is the rms velocity ($u = \sqrt{u_i^2}$).

The numerical resolution can be done with different fundamental approximate Riemman solvers. The Roe (Roe, 1981) and Jameson (Jameson et al., 1981) solvers, respectively based on upwind and central schemes, have been chosen for this work. For the Jameson solver, the chosen artificial dissipative coefficients are $k^{(2)}$=1 and $k^{(4)}$=0.032.

Motivated by the demand for very accurate CFD predictions at an ever-increasing level of detail ONERA has started the development of a new solver Aghora, based on high-order space time variational methods for unstructured polyhedral elements and mainly using Discontinuous Galerkin type methods (Renac et al., 2014, Chapelier et al., 2014). A number of finite volume schemes (Lax-Friedrichs, Roe, etc.) are available to approximate the convective fluxes across the element interfaces. The viscous fluxes can be discretized by using the BR2 scheme (Bassi et al., 1997) or the Symmetric Interior Penalty (SIP) method (Hartmann and Houston, 2008). We also performed the comparison with results from the Aghora solver.

Difficulties inherent in CFD :

Building the numerical simulation of the discrete form of PDEs is challenging when the objective is to reproduce accurately the analytical solution, provided that such a solution is known. Here two identified gaps have to be addressed. The first one concerns the right modeling choice about the fluid compressibility. The second gap concerns the numerical resolution at low Mach number. Whatever the choice of the PDE-type set is, its accurate resolution is challenging when the Mach number tends toward zero. This study is far from being exhaustive, considering the huge number of contributions in each of theses areas, but the two questions were addressed in this work.

The geometric symmetry is used to reduce the computational domain of the problem. As shown in Fig. 4 simulation was carried out in a quarter of the full domain, considering the symmetry in the four injection slots and assuming the same symmetry for the solution. Fig. 4 depicts a cross section of the simulation domain on which boundary conditions are specified.

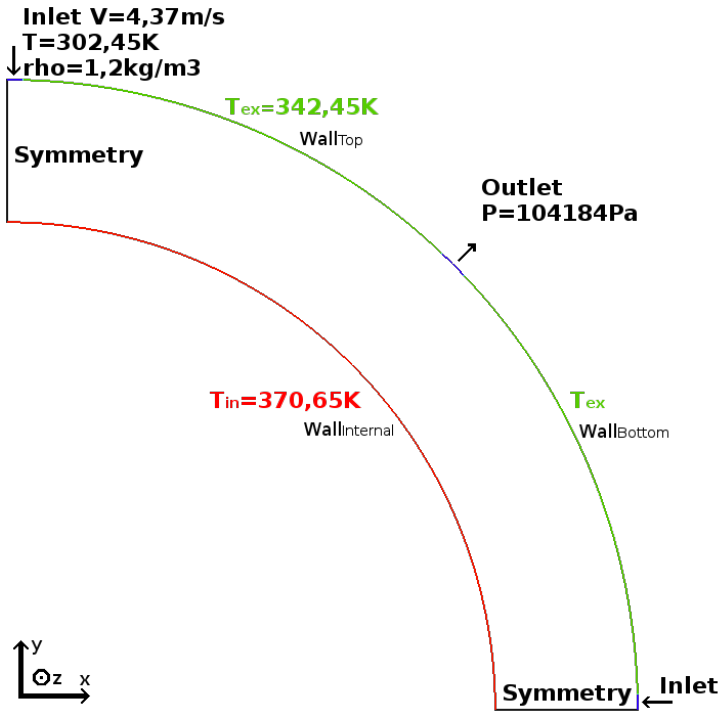

Figure 4: Cross section of the outflow configuration / Computational domain

From the experiment, the boundary conditions for FLUENT and *elsA* computations are given in Tab. 1.

Table 1. Physical boundary conditions.

Inlet, outlet and walls	
Density	1.2 $kg.m^{-3}$
Pressure	104 184.83 Pa
Inlet Temperature	302.45 K
Velocity magnitude	4.37 $m.s^{-1}$
Temperature - inner/heated wall	370.65 K
Temperature - external wall	342.45 K
Temperature - side walls	Linear between
(z=-0.0235m and z=0.0235m)	342.45K
	and 370.65K

The different options selected for the CFD with FLUENT and *elsA* appear in Tab. 2.

Table 2. Selected options with FLUENT and elsA.

	FLUENT (See FLUENT user's guide for more details)	*elsA* (See the User's reference manual of *elsA* for more details)
Inlet	Massflow_inlet Normal of inlets=(0, -1, 0) or (-1, 0, 0) mass flux=5.24 $kg.m^{-2}.s^{-1}$	Injmfr1 Normal of inlets=(0, -1, 0) or (-1, 0, 0) Surface mass flow=5.24 $kg.m^{-2}.s^{-1}$ Stagnation enthalpy=303 872.42 $m^2.s^{-2}$
Outlet	Pressure_outlet	Outpres
Internal wall (heated wall)	wall	wallisoth
External wall	wall	wallisoth

4. RESULTS

2D-3D comparisons with elsA+JamesonI
In the experiment, the height (*z* direction) of the cylindrical cavity (L=4.7cm) is comparable to the medium radius (7cm). 2D and 3D computations have been carried out in order to investigate the effect of finite height of the cylinder. The 3D mesh grid is composed of 726388 (229*52*61) nodes and 697680 quadrilateral cells (Fig. 5) build using 61 parallel planes along the z axis and reproducing in each plane the 2D mesh grid (11 628 cells in (*x,y*)). The plane z=0 is the plane of symmetry located in the middle of the height of the cylinder.
Histories of residues for both simulations, shown in Fig. 6 (2D) and 7 (3D), indicate that the 2D-3D-*elsA* computations have converged. The 3D computation time for 400000 iterations is about 13.5 CPU days using four processors.

Fig. 8 shows the 3D computed profiles of the wall heat-flux along three parallel arcs of a circle on the heated cylinder. The positions x=0 and x=0.084m correspond to the axis of two impacting jets and x=0.042m to the axis of an outlet slot. The profiles for z=-0.0195m and z=0.0195m overlap perfectly, indicating the symmetry of 3D simulations. The comparison (Fig. 9) between the 3D profile in the plane of symmetry and the profile obtained from 2D computations displays very similar shapes.

Flow streamlines obtained from 3D computations are plotted in Fig. 10 in the plane of symmetry (z=0) and the temperature variations are superimposed using a colour map. The flow and temperature patterns look the same as the results of 2D computations presented in Fig. 11. The good agreement between 2D and 3D computations in the vicinity of the plane of symmetry (z=0) leads us to conclude that 2D computations are relevant for further investigations using the FLUENT, *elsA* and Aghora numerical codes.

The errors on the total mass flow rate passing in the device, given in Tab. 3 and in Tab. 6, are less than 0,4% in relative value of the mass flow rate measured in the experiment. In Tab. 4 the convective heat transfer is 3.9% better in the case of *elsA*-3D than that of *elsA*-2D compared to experiment. Indeed there is only -1,4% of difference between the *elsA* -3D solution and the experiment against -5,3% when comparing the *elsA* -2D solutions with experiment.

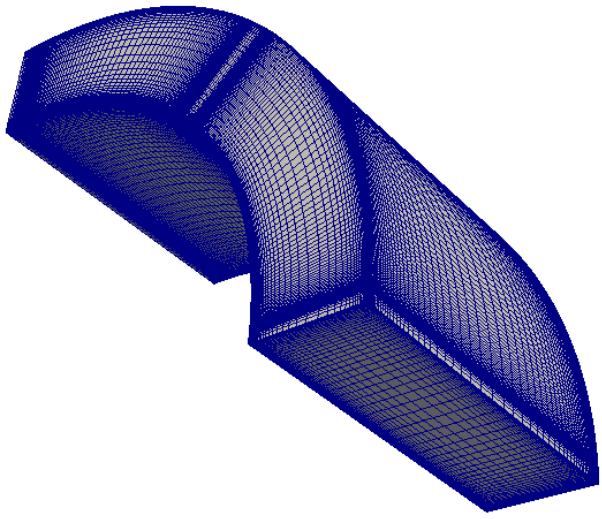

Figure 5: View of the 3D mesh

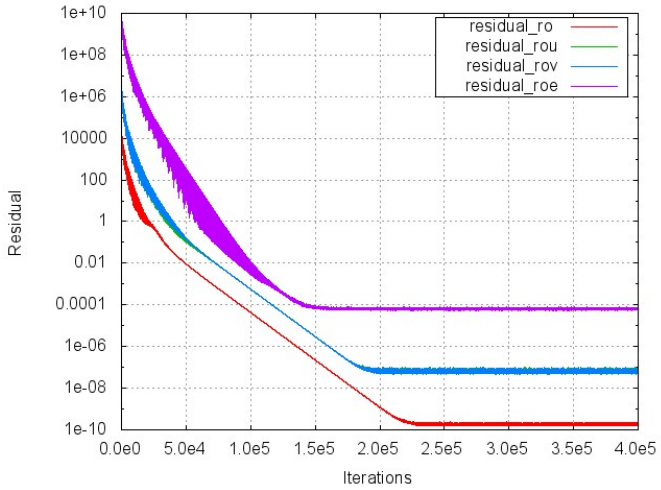

Figure 6: Evolution of residues during 2D computations with elsA.

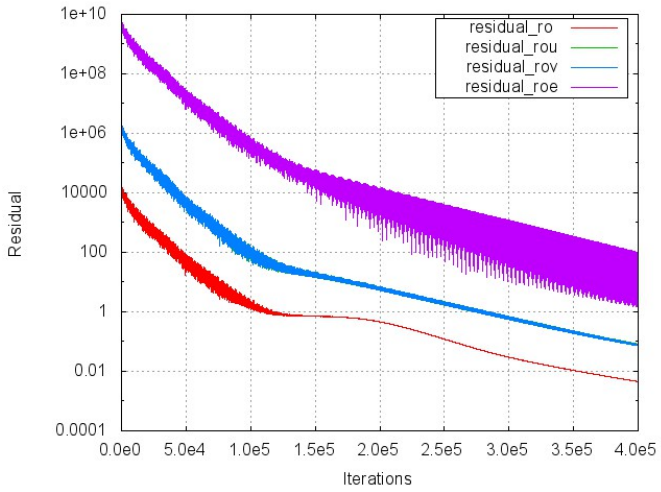

Figure 7: Evolution of residues during 3D computation with elsA.

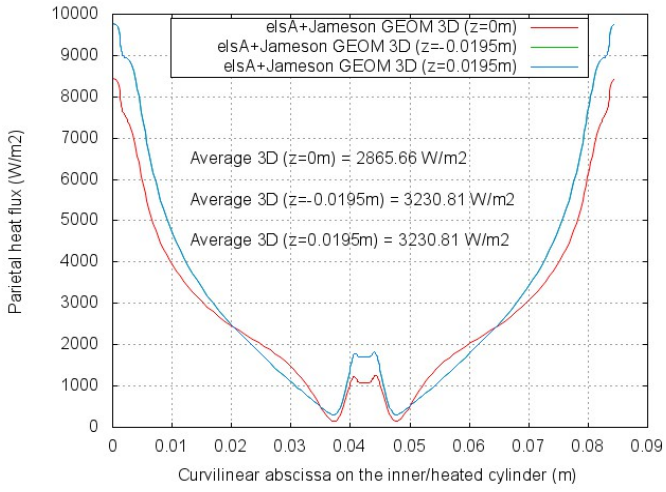

Figure 8: Comparison of heat-fluxes along arcs of circle on the inner-heated cylinder from 3D computations in three different planes.

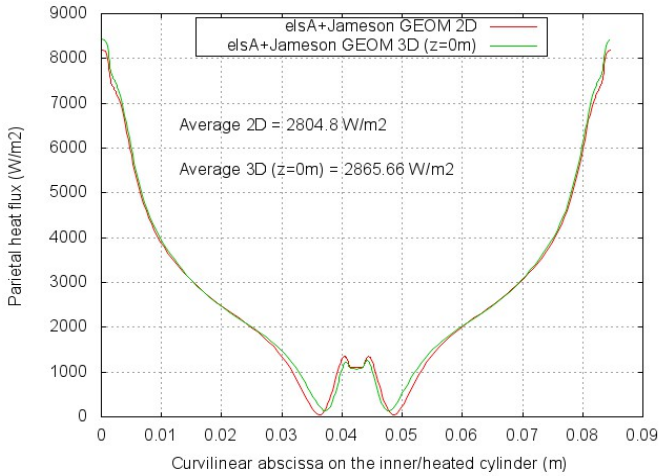

Figure 9: Comparison of heat-fluxes along an arc of circle on the inner-heated cylinder from 2D and 3D computations.

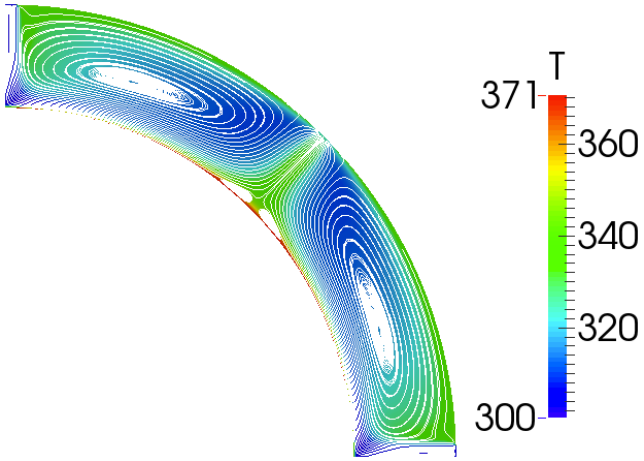

Figure 10: Flow streamlines superimposed on temperature variations. 3D computations with elsA+Jameson 3D. Result in plane z=0m.

Table 3. Error on the inlet/outlet mass flow rate with elsA 2D and elsA 3D.

	Experiment	*elsA 2D with Jameson*	*elsA* 3D with Jameson
Inlet mass flow rate ($kg.s^{-1}$)	0.000888	0.000884	0.000884
Error rate (over the experiment)		-0.4 %	-0.4 %
Outlet mass flow rate ($kg.s^{-1}$)	0.000888	0.000886	0.000887
Error rate (outlet over inlet)		0.2 %	0.3 %

Table 4. Convected heat flux comparisons with elsA 2D and elsA 3D. Experiment is the reference.

	Experiment	*elsA* 2D with Jameson	*elsA* 3D with Jameson
Convected heat flux (W)	20.00	18.93	19.72
Error rate (over the experiment)		-5.3 %	-1.4 %

2D-FLUENT-elsA 2D-computations

The same mesh grid has been used in this paper for all 2D computations made using the three models. Its properties are given in Tab. 5.
Figs. 11 to 13 show the streamlines and the temperature fields obtained with ANSYS-FLUENT and *elsA*. The main differences are observed in the eddy patterns generated in the annular domain. While the two *elsA* solutions in Figs. 11 and 12 look similar, the FLUENT-PISO solution in Fig. 13 displays a more complex eddy pattern. Moreover, although the boundary conditions of the simulation are steady, the FLUENT simulation shows slow spatial oscillations in time. Actually, the FLUENT solution does not converge, whichever the numerical method (SIMPLE or PISO) is used. As a consequence, the outlet mass flow rate and the convective heat flux vary in time. For FLUENT simulations Tab. 6 indicates that the relative error in the mass flow rate between outlet and inlet varies from -1,1% to 0,9% while for *elsA* the relative error (0,2% for Jameson and 0,3% for Roe) is stable. Tab. 7 indicates also that the convective heat flux obtained by the different models varies between -25,1% and -5,3% as compared to the experimental value. Again, the heat flux computed by *elsA* is stable, but it varies in time for the results obtained with FLUENT.

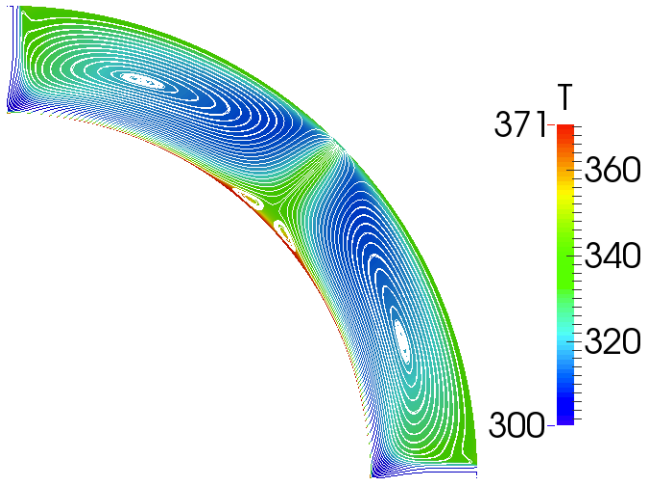

Figure 11: Flow streamlines superimposed on temperature variations. 2D computations with elsA+Jameson

Fig. 14 compares the heat flux along the heated cylinder obtained respectively with ANSYS-FLUENT and with the two *elsA* cases. Positions x=0 and x=0.084 correspond to the axes of two impacting jets and their respective heat fluxes are maximal, as expected. Starting from these extremities, fluxes globally decrease along the cylinder before increasing near the outlet slot axis. Looking at the Jameson and the PISO solutions, although the curve profiles are not strictly identical, the fluxes' average values are the same within 1.7%.

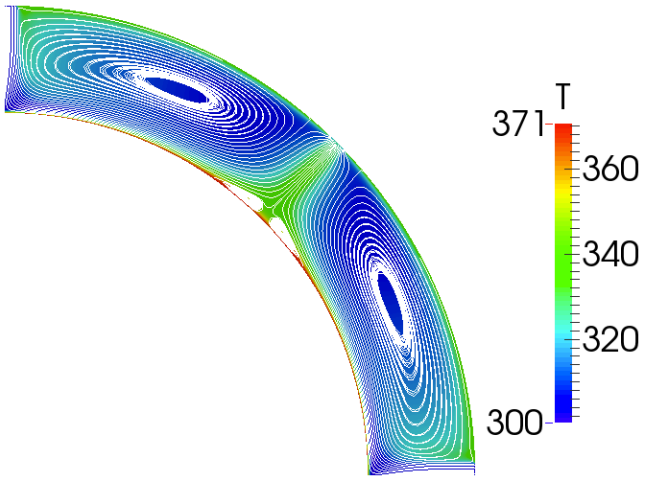

Figure 12: Flow streamlines superimposed on temperature variations. 2D computations with elsA+Roe.

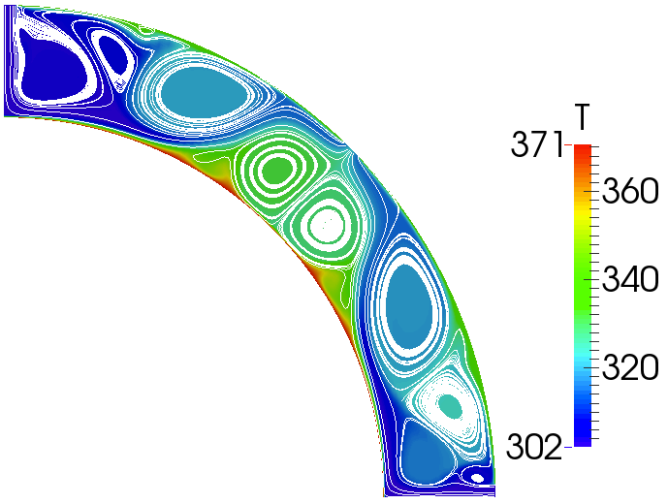

Figure 13: Flow streamlines superimposed on temperature variations. 2D computations with FLUENT+PISO (600 000 iters).

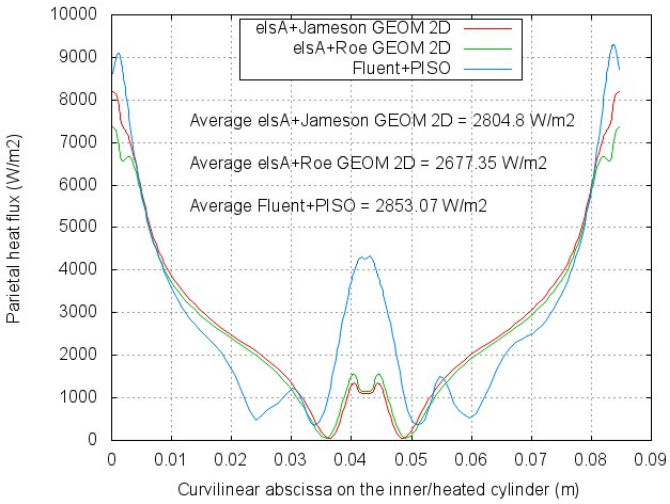

Figure 14: Comparison of heat-fluxes along an arc of circle on the inner-heated cylinder obtained from 2D computations (elsA and FLUENT).

Table 5. Grid mesh properties for FLUENT, elsA and AGHORA

	FLUENT, *elsA*, AGHORA
Number of points	11 908
Number of cells	11 628
Cell geometry	Quadrangular
Min and max edge size on the inner-heated cylinder (m)	$6.2e^{-5}$ to $1.1e^{-3}$
Min and max edge size on the outer cylinder (m)	$8.1e^{-5}$ to $1.4e^{-3}$

Table 6. Error on the inlet/outlet mass flow rate with FLUENT, elsA.

	Experiment	*FLUENT with SIMPLE*	*FLUENT with PISO*	***elsA** with Jameson*	***elsA*** with Roe
Inlet mass flow rate ($kg.s^{-1}$)	0.000888	0.000886	0.000886	0.000884	0.000884
Error rate (over the experiment)		-0.2 %	-0.2 %	-0.4 %	-0.4 %
Outlet mass flow rate ($kg.s^{-1}$)	0.000888	0.000878 to 0.000896	0.000883 to 0.000892	0.000886	0.000887
Error rate (outlet over inlet)		-1.1% to 0.9%	-0.5% to 0.4%	0.2 %	0.3 %

Table 7. Convected heat flux comparisons with FLUENT, elsA. Experiment is the reference.

	Experiment	*FLUENT with SIMPLE*	*FLUENT with PISO*	*elsA with Jameson*	***elsA*** with Roe
Convected heat flux (W)	20.00	15.17 to 16.48	14.98 to 16.43	18.93	16.85
Error rate (over the experiment)		-24.1% to -17.6%	-25.1% to -17.8%	-5.3 %	-15.7 %

2D-Aghora Computations

The 2D Aghora simulations use a nodal approach with polynomials of degree 1. The order of accuracy of the simulation is therefore 2^{nd}-order. We denote this simulation DG-p1. The boundary conditions (Tab. 8) are given in a different manner than specified for the previous 2D-computations (Tab. 3). For the Aghora simulations, the flow is driven by different pressure values at the inlet and outlet, whereas the mass flow rate was specified for the FLUENT and *elsA* simulations. At the inlet boundaries we impose constant values of the total pressure, total temperature, and the direction of the velocity, instead of the mass flow, the total temperature, and the direction of the velocity as is done in the previous 2D-simulations. This choice leads to an inlet mass flow that is smaller than the mass flow imposed in the experiment, and that imposed in the *elsA* and FLUENT computations. This is the reason why we cannot compare the convected heat flux obtained from the DG-p1 simulation with that provided by the experiment.

In this paragraph let us have a look at the comparison between the compressible modelings of Aghora and *elsA*. It is interesting to look at the temperature field and the streamlines pattern displayed by the DG-p1 simulation (Fig.15), as well as the heat flux distribution at the inner wall (Fig. 16). Indeed, from our experiment with the *elsA* code, for a given level of artificial dissipation in Jameson scheme, the overall features of the flow are not fundamentally affected by the two different ways of imposing the inlet condition. We can observe from Fig. 15 the very different behaviour between the results from the *elsA* simulations presented above and that from the DG-p1 simulation.

Table 8. Boundary conditions with AGHORA.

	AGHORA
Inlet	Pressure: 104196.29 Pa
	Temperature: 302.45 K
	Velocity direction: (0, -1, 0) or (-1, 0, 0)
Outlet	Pressure: 104 184.83 Pa
Internal wall	Temperature: 370.65 K
(heated wall)	Temperature: 342.45 K
External wall	

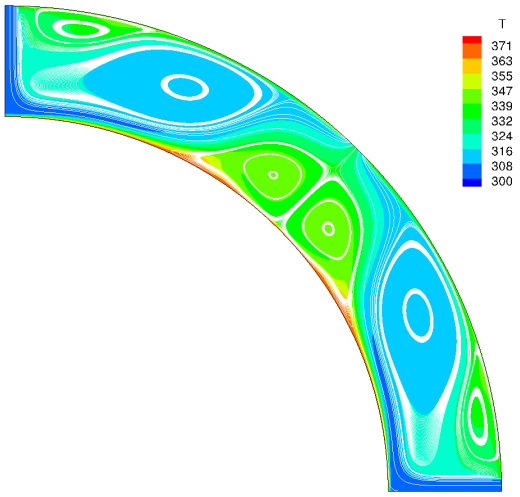

Figure 15: streamlines and temperature field for the DG-p1 simulation using Aghora.

The main difference lies in the much larger size of the two recirculation bubbles right below the outlet slot, as well as the appearance of two new secondary bubbles near the inlet slots. The authors believe that the reason for the significant differences found is the higher level of artificial dissipation selected in Jameson scheme in the *elsA* computation. Indeed, a number of numerical experiments using *elsA* and Aghora for different values of the artificial viscosity have demonstrated the strong sensitivity of the results to the accuracy of the numerical scheme. The differences in the flow patterns found between the *elsA* and the DG-p1 simulation have a direct effect on the profile of the wall heat-flux as seen from Fig. 16. A comparison with the profiles shown in Fig. 14, highlights the existence of a more intense heat exchange in the vicinity of the outlet axis. The maximum level of heat-flux found in the DG-p1 simulation appears to be lower than that found in the other simulations. This is a logical consequence of the lower level of mass flow present in the DG-p1, as mentioned above, which leads to a reduction of the overall heat-exchange in the cooling cavity.
As surprising as it might seem, the result of Aghora shares a closer similarity with the result of FLUENT obtained by the incompressible modeling. Comparing the eddy patterns of Figs. 13 and 15 both have the two recirculation bubbles right below the outlet slot. Moreover looking at Figs 14 and 16, the behaviours of the wall heat-flux looks the same even if the levels are different.

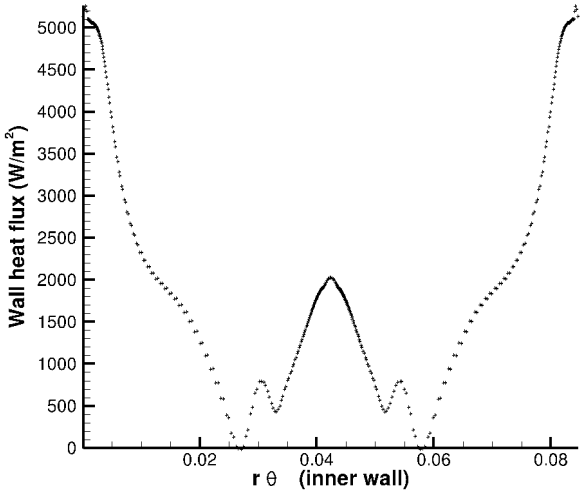

Figure 16: Profile of heat flux at the inner wall along the azimuthal direction. DG-p1 simulation using Aghora.

5. CONCLUSION AND PERSPECTIVES

In the context of onboard green aircraft projects, the increasing use of electrical engines requires more efficient cooling systems. This study presents the results of a comparative study of simulations by various incompressible or compressible CFD models of the convective heat transfer achieved by impacting jets. The test case is given by a specific laboratory experiment, which is devoted at the university of Pau to the study of cooling of small-sized turbo engines.

Comparisons between the results from 3D and 2D computations support the relevance of 2D models for simulating the convective heat transfer by the impacting jets as carried out in the experiment.

The present study focuses on low Reynolds number confined flow conditions. A comparison is made between the results of numerical simulations obtained using incompressible models of FLUENT and the compressible ones of *elsA* and Aghora. The flow fields obtained by the three codes show eddy patterns in the simulated annular domain, which differ in detail.

Even though the boundary conditions are steady, the results obtained with the incompressible models of FLUENT display instabilities while the compressible models of *elsA* are stable with residuals which seem to converge. Thus the parietal heat-flux distributions along the inner wall, predicted by the different models, display differences. Nevertheless, the average of these fluxes are the same within less than 2%. For this flow condition the global convective heat fluxes computed with FLUENT and *elsA* are ranging from 0.75 to 0.95 of the experimental data. In such a CFD case, the flow stability seems to be a key issue linked with the compressibility effects.

A second-order DG simulation has also been performed with a lower inlet mass rate using the Aghora compressible solver, by setting the polynomial degree to 1 (DG-p1) and using the same mesh resolution as in previous 2D-simulations. The solutions from the two compressible solvers (i.e. *elsA* and Aghora) appear to be fundamentally different. Concerning the Jameson scheme, the authors believe that the significant difference found results from the higher level of artificial dissipation selected in Jameson scheme for the *elsA* computations. This has a direct effect on the profile of the wall heat-flux, for which the existence of a more intense heat exchange in the vicinity of the outlet axis is observed for the DG-p1 simulation. As the inlet mass flow rate is slightly lower (in the case of Aghora) compared to those used in *elsA* and FLUENT, it is not surprising that the level of the wall heat-flux is also lower. However, as observed in the eddy pattern, the heat flux profile obtained by Aghora looks rather the same than that provided by the incompressible modeling with FLUENT.

A new boundary condition with imposition of the mass flow is being implemented in the Aghora solver and new simulations are planned in order to verify the conclusions of this preliminary analysis. It would also be of great interest to perform higher-order simulations using Aghora (at least p=2 and p=3). Indeed, one of the

remarkable properties of high-order methods is the little influence of the selected numerical flux (convective and viscous) on the accuracy of the solution.

It is encouraging that the results of simulations are in qualitative agreement with the laboratory experiments and recover the order of magnitude of the total heat transfer measured. Nevertheless, much remain to be done. Modeling compressible fluid flows is known to be difficult for low Mach number conditions. Our goal is orient ourselves into the development of "All Mach" solvers.

ACKNOWLEDGMENTS

The authors thank University of Pau, Conseil Régional d'Aquitaine and SAFRAN-Turbomeca for their financial support to this work. N. Lantos is acknowledged for his invaluable and daily help in the best use as possible of the *elsA* software. For her useful help with producing the gmsh mesh used in the Aghora simulation, the authors wish to express their gratitude to M.-C. Le Pape from ONERA. Part of this research got public financial support from the DGE (Direction Générale des Entreprises) after having been selected by the French clusters Aerospace Valley, ASTech and PEGASE.

REFERENCES

- F. Bassi, S. Rebay, G. Mariotti, S. Pedinotti and M. Savini, A High-order accurate discontinuous finite element method for inviscid and viscous turbomachinery Flows, In proceedings of the 2nd European Conference on Turbomachinery Fluid Dynamics and Thermodynamics, R. Decuypere, G. Dibelius (eds.), Antwerpen, Belgium, 1997.
- L. Cambier, S. Heib, and S. Plot. The ONERA *elsA* CFD software : input from research and feedback from industry. *Mechanics & Industry*, 14(03), pp.159–174, 2013.
- J.-B. Chapelier, M. de la Llave Plata, F. Renac, and E. Lamballais. Evaluation of a high-order discontinuous Galerkin method for the DNS of turbulent flows. Comput. Fluids, 95 (2014), pp. 210-226
- R. Gardon, J.C. Akfirat, The role of turbulence in determining the heat-transfer characteristics of impinging jets, Int. J. Heat Mass Transfer 8 (1965) 1261-1272.
- H. Martin, Heat and mass transfer between impinging gas jets and solid surfaces, Adv. Heat Transfer 13 (1977) 1-60.
- F. Gori, L. Bossi, On the cooling effect of an air jet along the surface of a cylinder, International Communications in Heat and Mass Transfer 27 (2000) 667–676.
- R. Hartmann and P. Houston, An optimal order interior penalty discontinuous Galerkin discretization of the compressible Navier-Stokes equations J. Comput. Phys. 227 (2008), pp. 9670-9685.
- K. Jambunathan, E. Lai, M.A. Moss, B.L. Button, A review of heat transfer data for single circular jet impingement, Int. J. Heat Fluid Flow 13 (1992) 106-115.
- Gardon R, Akfirat J. 1966. Heat transfer characteristics of impinging two-dimensional air jets. J Heat Transf 88:101–8.
- A. Jameson, W. Schmidt, and E. Turkel. Numerical Solution of the Euler Equations by Finite Volume Methods using Runge–Kutta Stepping Schemes. Technical Report 81–1259, AIAA, 1981.
- Franklyn J. Kelecy. Coupling momentum and continuity increases CFD robustness, ANSYS advantage, volume II, issue 2, 2008.
- M. de la Llave Plata, V. Couaillier, C. Marmignon, M.C. Le Pape, M. Gazaix, B. Cantaloube, "Further developments in the multiblock hybrid CFD solver *elsA*-H", AIAA paper 2012-1112
- C.S. McDaniel, B.W. Webb, Slot jet impingement heat transfer from circular cylinders, International Journal of Heat and Mass Transfer 43 (2000) 1975-1985.
- F. Renac, M. de la Llave Plata, E. Martin, J.-B. Chapelier, and V. Couaillier, Aghora : A High-Order DG Solver for Turbulent Flow Simulations. IDIHOM : Industrialization of High-Order Methods - A

Top-Down Approach, Notes on Numerical Fluid Mechanics and Multidisciplinary Design, N. Kroll, C. Hirsch, F. Bassi, C. Johnston, and K. Hillewaert, 128 (2014) pp. 315-335, Springer.

- P. L. Roe. Approximate Riemann Solvers, Parameter Vectors, and Difference Schemes. J. Comput. Phys., 43:357–372, 1981.
- D. Singh, B. Premachandran, Sangeeta Kohli, Experimental and numerical investigation of jet impingement cooling of a circular cylinder, International Journal of Heat and Mass Transfer 60 (2013) 672–688.
- D. Singh, B. Premachandran, S. Kohli, Circular air jet impingement cooling of a circular cylinder with flow confinement, International Journal of Heat and Mass Transfer 91 (2015) 969–989.
- D. Singh, B. Premachandran, S. Kohli, Effect of nozzle shape on jet impingement heat transfer from a circular cylinder, International Journal of Thermal Sciences 96 (2015) 45-69.
- X.L. Wang a, D. Motala b, T.J. Lu a, S.J. Song c, T. Kim b, Heat transfer of a circular impinging jet on a circular cylinder in crossflow, International Journal of Thermal Sciences 78 (2014) 1-8.
- N. Zuckerman, N. Lior, Jet impingement heat transfer: physics, correlations, and numerical modeling, Adv. Heat Transf. 39 (2006) pp.565-631.
- N. Zuckerman, N. Lior, Radial slot jet impingement flow and heat transfer on a cylindrical target, Journal of Thermophysics and Heat Transfer 21 (3) (2007) 548–561.